JOURNAL OF THERMOPHYSICS AND HEAT TRANSFER
Vol. 8, No. 3, July–Sept. 1994

Analysis of Forced Convection Enhancement in a Channel Using Porous Blocks

P. C. Huang* and K. Vafai†
Ohio State University, Columbus, Ohio 43210

This work presents a detailed investigation of forced convection enhancement in a channel using multiple emplaced porous blocks. The Brinkman-Forchheimer-extended Darcy model is used to characterize the flowfield inside the porous regions in order to account for the inertia effects as well as the viscous effects. Solution of the coupled governing equations for the porous/fluid composite system is obtained using a stream function-vorticity approach. Important fundamental and practical results have been presented and discussed. These results thoroughly document the dependence of the streamline, isotherm, and local Nusselt number distributions on the governing parameters defining the problem, such as the Reynolds number, Darcy number, Prandtl number, inertial parameter, and two pertinent geometric parameters. An in-depth discussion of the formation and variation of the recirculation caused by the porous medium is presented, and the existence of an optimum porous matrix is demonstrated. It is shown that altering some parametric values can have significant and interesting effects on both the flow pattern as well as heat transfer characteristics.

Nomenclature

A = dimensionless geometric parameter, W^*/H^*
B = dimensionless geometric parameter, D^*/W^*
D = spacing between blocks, m
Da = Darcy number, K/L^2
F = function used in expressing inertia terms
H = height of the porous blocks, m
h = convective heat transfer coefficient, W/m^{2}K
K = permeability of the porous medium, m^2
k = thermal conductivity, W/mK
L = length of the channel as shown in Fig. 1a, m
l_1 = length of the channel upstream of the blocks, m
l_2 = length of the channel downstream of the blocks, m
N = number of blocks
Nu = Nusselt number
Pe = Peclet number, $u_\infty L/\alpha$
Pr = Prandtl number, ν/α
R = height of channel
Re = Reynolds number, $u_\infty L/\nu$
T = temperature, K
u = x-component velocity, m/s
v = velocity vector, m/s
W = width of the porous block, m
x = horizontal coordinate, m
y = vertical coordinate, m
α = thermal diffusivity, m^2/s
α_{eff} = effective thermal diffusivity, $k_{\text{eff}}/\rho_f c_{p,f}$, m^2/s
Δx = x-direction width of the control volume
Δy = y-direction width of the control volume
δx = distance in the x direction between two adjacent grid points
δy = distance in the y direction between two adjacent grid points
ε = porosity of the porous medium
θ = dimensionless temperature, $(T - T_0)/(T_w - T_0)$
Λ = inertial parameter, $FL\varepsilon/\sqrt{K}$
μ = dynamic viscosity, kg/ms
ξ = vorticity
v = y-component velocity, m/s
Φ = transported property; general dependent variable
Ψ = stream function

Subscripts
av = average
eff = effective
f = fluid
I = interface
m = bulk mean
p = porous
x = local
w = wall
0 = condition at inlet

Superscript
* = dimensionless quantity

Received March 8, 1993; revision received June 3, 1993; accepted for publication June 4, 1993.

*Graduate Student, Department of Mechanical Engineering.
†Professor, Department of Mechanical Engineering. Member AIAA.

Introduction

FORCED convection heat transfer in a channel or duct fully or partially packed with a porous material is of considerable technological interest. This is due to the wide range of applications such as direct contact heat exchangers, electronic cooling, heat pipes, etc. It has been demonstrated that insertion of a high-conductivity porous material in a cooling passage can have a positive effect on convective cooling. Koh and Colony[1] performed a numerical analysis of the cooling effectiveness of a heat exchanger containing a conductive porous medium, while Koh and Stevens[2] conducted an experimental investigation for the same problem. It was shown that for the case of a fixed wall temperature the heat flux at the channel wall can be increased by over three times by using a porous material in the channel. Rohsenow and Hartnett[3] presented a constant Nusselt number for the fully developed region in a porous medium bounded by two parallel plates, based on the Darcy flow model. To account for the effect of a solid boundary, Kaviany[4] performed a numerical study of laminar flow through a porous channel bounded by isothermal plates based on the generalized model developed in Vafai and Tien.[5] Poulikakos and Renken[6] have investigated the effect of flow inertia, variable porosity, and a solid boundary on the fluid flow and heat transfer through porous media bounded

by constant-temperature parallel plates and a circular pipe. They found that boundary and inertial effects decrease the Nusselt number where variable porosity effects increase the Nusselt number.

The above-referenced investigations were based on filling the entire channel with a porous medium. This method, while beneficial in augmenting the heat transfer rate, can significantly increase the pressure drop inside the channel. Furthermore, the results of those investigations cannot be extended to parts of other applications such as electronic cooling, fin configurations, solidification of castings, and geothermal applications. An important and fundamental problem in heat transfer augmentation in a channel is related to forced convection through a channel with multiple porous emplaced blocks. The flow over the fluid region is governed by the Navier-Stokes equation, and the flow through the fluid-saturated porous medium is governed by a volume-averaged generalized momentum equation which is referred to as the Brinkman-Forchheimer-extended Darcy model.[6] These two flows are coupled through the interface boundary conditions at the porous/fluid interface. The interactions of flow and temperature fields between the porous-saturated region and the fluid region have a significant influence on the convection phenomenon in these systems. Several investigations were devoted to the problem of finding the proper set of boundary conditions at the interface between a fluid flow in a porous medium and the adjacent region without a porous medium. Beavers and Joseph[7] experimentally reported the mass efflux of a poiseuille flow over a naturally permeable medium based on Darcy's law. They found that when a viscous fluid passes through a porous solid, tangential stress entrains the fluid below the interface with a velocity which is slightly greater than that of the fluid in the bulk of the porous medium. Levy and Sanchez-Palencia[8] found that when the typical length scale of the external flow is large compared with the microscopic scale, the velocity field transition at the interface from the porous media to the free fluid region occurs over a thin region of the order of the pore scale. They also showed that depending on the direction of the pressure gradient in the porous medium, two different kinds of phenomena may appear at the interface.

Due to the mathematical difficulties in simultaneously solving the coupled momentum equations for both the porous and fluid regions, very little work has been done on internal forced convection on the porous/fluid composite system. Vafai and Thiyagaraja[9] have performed an analytical investigation of a fully developed forced convection for three basic types of interface composites. They obtained analytical solutions for the velocity and temperature distributions as well as analytical expression for the Nusselt numbers for all three classes of interface composites investigated in their work. Poulikakos and Kazmierczak[10] have presented a theoretical study of forced convection in a channel with a porous region attached at its wall, based on the Brinkman-extended Darcy model. Some features of the heat transfer enhancement in a narrow flow passage was investigated by Ichimiya and Mitsushiro.[11]

In the present study, a numerical investigation of forced convection in a parallel plate channel with porous blocks emplaced at the bottom wall is presented. The analysis is based on the use of Brinkman-Forchheimer-extended Darcy model in the porous media and the Navier-Stokes equation in the fluid region. The use of the porous medium generally enhances the mixing within the fluid region resulting in a higher heat transfer than that obtained in the corresponding smooth channel. In the present investigation the basic interaction phenomena between the porous substrate and the fluid region for these types of composite systems as well as the methodology for enhancing the heat transfer rate within the channel have been analyzed. Furthermore, the effects of various parameters governing the hydrodynamic and thermal characteristics of the problem are analyzed.

Analysis

A schematic diagram of forced convection enhancement in a channel using porous blocks is displayed in Fig. 1a. The fluid enters at ambient temperature T_0, with a parabolic ve-

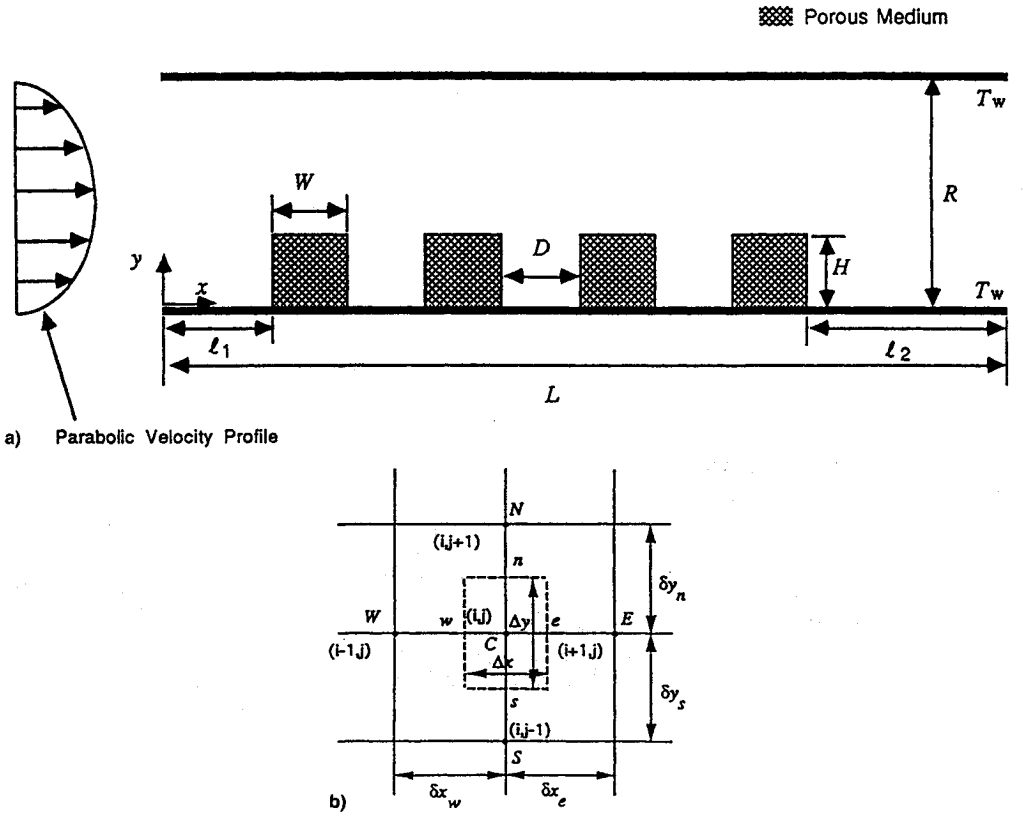

Fig. 1 Schematic diagram of a) force convection in a parallel plate channel with porous block obstacles and b) grid system for the computational domain.

locity profile. The plate walls are maintained at constant T_w. The flow is assumed to be steady, incompressible and two-dimensional. In addition, the thermophysical properties of the fluid and the porous matrix are assumed to be constant, and the porous medium is considered homogeneous, isotropic, nondeformable, and in local thermodynamic equilibrium with the fluid. In this study, the Brinkman-Forchheimer-extended Darcy model, which accounts for the effects of inertia as well as friction caused by macroscopic shear,[6,12] is used to demonstrate the flow inside the porous region. The equations governing momentum and energy conservation for the present problem will be separately written for the porous and fluid regions in dimensionless forms.

For the porous region

$$u_p^* \frac{\partial \xi_p^*}{\partial x^*} + v_p \frac{\partial \xi_p^*}{\partial y^*} = \frac{1}{Re_{\text{eff}}} \nabla^2 \xi_p^* - \frac{1}{Re_{\text{eff}} Da} \xi_p^* - \Lambda |v_p^*| \xi_p^* - \Lambda \left(v_p^* \frac{\partial |v_p^*|}{\partial x^*} - u_p^* \frac{\partial |v_p^*|}{\partial y^*} \right) \tag{1}$$

$$\nabla^2 \Psi_p^* = -\xi_p^* \tag{2}$$

$$u_p^* \frac{\partial \theta_p}{\partial x^*} + v_p^* \frac{\partial \theta_p}{\partial y^*} = \frac{1}{Pe_{\text{eff}}} \nabla^2 \theta_p \tag{3}$$

Note that the field variables in the porous region are volume-averaged quantities as described by Vafai and Tien.[6] The approach here is based on Vafai and Tien[6] in which the shape of the averaging volume is chosen for physical interpretation of the relevant averaged quantities. In effect, our averages will correspond to the line averages of the physical quantities in the transverse direction. Therefore, our results are valid (as mentioned in Vafai and Tien[6]) for a two-dimensional flow. By choosing a cylindrical volume, one can satisfy the criteria for selecting three distinctive length scales in a porous media, i.e.,

$$d \ll h \ll L$$

where d is some microscopic characteristic length which is representative of the distance over which significant variations in the point velocity takes place, h a characteristic length for the averaging volume, and L is some macroscopic characteristic dimension representative of the process under consideration.

For the fluid region

$$u_f^* \frac{\partial \xi_f^*}{\partial x^*} + v_f^* \frac{\partial \xi_f^*}{\partial y^*} = \frac{1}{Re_f} \nabla^2 \xi_f^* \tag{4}$$

$$\nabla^2 \Psi_f^* = -\xi_f^* \tag{5}$$

$$u_f^* \frac{\partial \theta_f}{\partial x^*} + v_f^* \frac{\partial \theta_f}{\partial y^*} = \frac{1}{Pe_f} \nabla^2 \theta_f \tag{6}$$

where the operator ∇^2 is the Laplacian. The following dimensionless variables used in Eqs. (1–6) are defined as

$$x^* = \frac{x}{R}, \quad y^* = \frac{y}{R}, \quad u^* = \frac{u}{u_{\text{av}}}, \quad v^* = \frac{v}{u_{\text{av}}}, \quad |v^*| = \sqrt{u^{*2} + v^{*2}} \tag{7}$$

$$Pe_{\text{eff}} = \frac{u_{\text{av}} R}{\alpha_{\text{eff}}}, \quad Pe_f = \frac{u_{\text{av}} R}{\alpha_f}, \quad Re_{\text{eff}} = \frac{u_{\text{av}} R}{\nu_{\text{eff}}}, \quad Re_f = \frac{u_{\text{av}} R}{\nu_f} \tag{8}$$

$$Da = \frac{K}{R^2}, \quad \Lambda = \frac{FR\varepsilon}{K^{1/2}}, \quad \Psi^* = \frac{\Psi}{u_{\text{av}} R}, \quad \xi^* = \frac{R\Psi}{u_{\text{av}}}, \quad \theta = \frac{T - T_0}{T_w - T_0} \tag{9}$$

The stream function and vorticity are defined in the usual way

$$u = \frac{\partial \Psi}{\partial y}, \quad v = -\frac{\partial \Psi}{\partial x} \tag{10}$$

$$\xi = \frac{\partial v}{\partial x} - \frac{\partial u}{\partial y} \tag{11}$$

The appropriate boundary conditions for the present problem are

1) at $x^* = 0$, $0 < y^* < 1$ (the inlet)

$$u^* = 6y^*(1 - y^*), \quad v^* = 0$$

$$v, \xi^* = 6(1 - 2y^*)$$

$$\theta = 0$$

2) at $x^* = L^*$, $0 < y^* < 1$ (the exit)

$$\int_0^1 u^* \, dy^* = 1, \quad v^* = 0$$

$$\frac{\partial \Psi^*}{\partial x^*} = 0, \quad \frac{\partial \xi^*}{\partial x^*} = 0, \quad \frac{\partial \theta^*}{\partial x^*} = 0$$

3) at $0 < x^* < L^*$, $y^* = 1$ (upper plate)

$$u^* = 0, \quad v^* = 0, \quad \Psi^* = 1$$

$$\xi^* = -\frac{\partial^2 \psi^*}{\partial y^{*2}}, \quad \theta = 1$$

4) at $0 < x^* < L^*$, $y^* = 0$ (bottom plate)

$$u^* = 0, \quad v^* = 0, \quad \Psi^* = 0$$

$$\xi^* = -\frac{\partial^2 \Psi^*}{\partial y^{*2}}, \quad \theta = 0$$

The above boundary conditions correspond to a fluid entering the domain with a fully developed profile, along with the application of the no-slip condition on the two parallel walls. At the channel exit, axial diffusion is set equal to zero to satisfy the closure for the elliptic problem, and u is calculated to satisfy conservation of mass. The exit boundary conditions were evaluated very carefully by choosing two different regions corresponding to the physical and computational domains. The location of the exit boundary condition was systematically moved further downstream until it was ensured that the exit boundary condition has no detectable effect on the physical domain. The upper and bottom plates of the channel are maintained at a constant temperature.

At the porous/fluid interface, the following quantities evaluated in both the porous and fluid regions are matched: horizontal and vertical velocities, normal and shear stresses, temperature, pressure, and heat flux. The matching conditions for the present governing equations can be expressed as

$$\Psi_p^* = \Psi_f^*, \quad \xi_p^* = \xi_f^*, \quad \theta_p^* = \theta_f^*$$

Based on the above coupled governing equations, boundary conditions, and the shape of porous/fluid interface, it is seen

that the present problem is governed by six dimensionless parameters. These are the Darcy, Reynolds, two Prandtl numbers, inertia parameter, and A and B, where

$$A = \frac{W^*}{H^*}, \qquad B = \frac{D^*}{W^*}$$
$$H^* = \frac{H}{R}, \qquad D^* = \frac{D}{R}, \qquad W^* = \frac{W}{R} \tag{12}$$

To evaluate the effects of the porous material on the heat transfer rate at the wall, the local Nusselt number is evaluated as follows:

$$Nu_x = \frac{hR}{k_f} = -\frac{k_{\text{eff}}(T_w - T_0)}{k_f(T_w - T_m)} \frac{\partial\theta}{\partial y^*}\bigg|_{y^*=0}$$
$$= -\frac{k_{\text{eff}}}{k_f} \frac{1}{(1 - \theta_m)} \frac{\partial\theta}{\partial y^*}\bigg|_{y^*=0} \tag{13}$$

where $\theta_m = (T_m - T_0)/(T_w - T_0)$ is the dimensionless form of T_m defined by

$$T_m = \frac{\int_0^R |u| T \, dy}{\int_0^R |u| \, dy} \tag{14}$$

Here, the absolute value of the velocity is used as in Kelkar and Patankar[13] so that the regions of recirculating flow are properly represented. Note that the definition of the Nusselt number, based on the conductivity of the fluid, permits a direct comparison between the smooth and blocked channels.

Numerical Method

To obtain the solution of the foregoing system of equations, the region of interest is overlaid with a variable grid system. Applying the central differencing for the diffusion terms and a second upwind differencing for the convective terms, the finite difference forms of the vorticity transport, stream function, and energy equations were derived by a control-volume integration of these differential equations over discrete cells surrounding any given grid point, as shown in Fig. 1b. This results in a system of equations of the following form:

$$C_C\Phi_C = C_N\Phi_N + C_S\Phi_S + C_E\Phi_E + C_w\Phi_W + S^\Phi \tag{15}$$

where Φ stands for the transport variables, C are coefficients combining convective and diffusive terms, and S^Φ is the appropriate source term. The subscripts on C denote the main grid points surrounded by the four neighboring points denoted as N, S, E, and W. The finite difference equations for ξ^*, Ψ^*, and θ obtained in this manner were solved by the extrapolated-Jacobi scheme. This iterative scheme is based on a double cyclic routine, which translates into a sweep of only half of the grid points at each iteration step.[14] The numerical procedure for solving the finite difference equations is as follows: 1) overlay the computational domain with a variable mesh; 2) assign values of Ra, Da, Λ, A, B, and initial values for ξ^*, Ψ^*, u, v, and θ in Eqs. (1–6), and the corresponding boundary conditions; 3) calculate the new values of ξ^* at each node by using the finite difference set of equations for ξ^* as given by Eq. (15); 4) calculate the new values of Ψ^* at each node from Eq. (15) for Ψ^* by using the values of ξ^* found from step 3; 5) calculate the new values of the velocity from $u = \Psi_y^*$ and $v = -\Psi_x^*$; 6) update new boundary values using the new nodal values for Ψ^* and ξ^*; 7) repeat steps 3–6, until the following convergence criteria is satisfied:

$$\max \left| \frac{\phi_{i,j}^{n+1} - \phi_{i,j}^n}{\phi_{i,j}^n} \right| < 10^{-6} \tag{16}$$

where ϕ stands for ξ^*, Ψ^*, or θ and n denotes the iteration number; 8) calculate θ by using the finite difference set of equations for θ as given by Eq. (15) with the assigned values of Pr and the values of Ψ^* obtained from step 7, until the criterion of convergence for θ is satisfied.

The interfacial properties play very important roles in the porous/fluid composite system. This is due to the abrupt change of thermophysical properties, such as the viscosity, permeability, porosity, and the thermal conductivity, across the interface. These effects on the porous/fluid interface are represented by the nondimensional parameters Re, Da, Λ , and Pr. The harmonic mean formulation recommended by Patankar[15] was used to treat these discontinuous characteristics at the porous/fluid surface. This ensured the continuity of the convective and diffusive fluxes across the interface without requiring the use of an excessively fine grid structure. For the present case Re, Da, Λ, and Pr at the interface of a control volume were found as

$$Re_I = \frac{2Re_{\text{eff}}Re_f}{Re_{\text{eff}} + Re_f}, \qquad Da_I = \frac{2Da_{\text{eff}}Da_f}{Da_{\text{eff}} + Da_f}$$
$$Da_I = \frac{2Da_{\text{eff}}Da_f}{Da_{\text{eff}} + Da_f}, \qquad Pr_I = \frac{2Pr_{\text{eff}}Pr_f}{Pr_{\text{eff}} + Pr_f} \tag{17}$$

Instead of the momentum equations in Eqs. (1) and (4), the following were used across the interface:

$$u_p^* \frac{\partial\xi_p^*}{\partial x^*} + v_p^* \frac{\partial\xi_p^*}{\partial y^*} = \frac{1}{Re_I} \nabla^2\xi_p^* + S_p^* \tag{18a}$$

where

$$S_p^* = -\frac{1}{Re_I Da_I} \xi_p^* - \Lambda_I |v_p^*| \xi_p^* - \Lambda_I \left(v_p^* \frac{\partial |v_p^*|}{\partial x^*} - u_p^* \frac{\partial |v_p^*|}{\partial y^*} \right) + \frac{u_p^*}{Re_I} \frac{\partial}{\partial y^*} \left(\frac{1}{Da_I} \right) - \frac{v_p^*}{Re_I} \frac{\partial}{\partial x^*} \times \left(\frac{1}{Da_I} \right) + |v_p^*| u_p^* \frac{\partial}{\partial y^*} (\Lambda_I) - |v_p^*| v_p^* \frac{\partial}{\partial x^*} (\Lambda_I) \tag{18b}$$

$$u_f^* \frac{\partial\xi_f^*}{\partial x^*} + v_f^* \frac{\partial\xi_f^*}{\partial y^*} = \frac{1}{Re_I} \nabla^2\xi_f^* + S_f^* \tag{19a}$$

where

$$S_f^* = \frac{u_f^*}{Re_I} \frac{\partial}{\partial y^*} \left(\frac{1}{Da_I} \right) - \frac{v_f^*}{Re_I} \frac{\partial}{\partial x^*} \left(\frac{1}{Da_I} \right) + |v_f^*| u_f^* \frac{\partial}{\partial y^*} (\Lambda_I) - |v_f^*| v_f^* \frac{\partial}{\partial x^*} (\Lambda_I) \tag{19b}$$

where Eqs. (18a) and (18b) are for the porous side, and Eqs. (19a) and (19b) are for the fluid side of the interface. Note that constant values of Da, and Λ were used for a specified porous substrate. In the present work, due to lack of other information, the effective viscosity of the fluid-saturated porous medium is set equal to the fluid viscosity. It has been found that this approximation provides a good agreement with experimental data.[16,17]

The vorticity at the wall is evaluated using the linear Taylor series approximation, that is

$$\xi_p^* = -\left[\frac{3(\Psi_{\text{np}}^* - \Psi_p^*)}{\Delta y_{\text{np}}^2} + \frac{\xi_{\text{np}}^*}{2} \right]$$

where the subscript np denotes the first neighboring point next to the boundary and Δy_{np} represents the normal distance from the wall to the point np.

In this study, the computational domain was chosen to be larger than the physical domain to eliminate the entrance and exit effects and to satisfy continuity at the exit. A systematic set of numerical experiments was performed to ensure that the use of a fully developed velocity profile for the outflow boundary condition has no detectable effect on the flow solution within the physical domain. That is, the downstream length beyond the physical domain was determined by trial and error to ensure that the effects of the outflow boundary condition were well outside of the physical domain.

A nonuniform grid system with a large concentration of nodes in regions of steep gradients, such as those close to the walls and porous blocks, was employed. A grid independence test showed that there is only a very small difference (less than 1%) in the streamlines and isotherms among the solutions for 218×69, 258×158, and 300×69 grid distributions. As this difference is small, our computations in this work were based on a 218×69 grid system. These computations, performed on a Cray Y-MP, took about 300–500 CPU seconds depending upon the different governing parameters.

To validate the numerical scheme used in the present study, comparisons with two relevant results were made. These comparisons were carried out for the problem of hydrodynamically fully developed forced convection in a channel with a porous medium partially covering the external boundary,[10] and external forced convection over a flat plate embedded in a porous medium (i.e., $H^* \to \infty$ and $W^* \to \infty$), representing the full porous medium case.[9] The result of these comparisons (being similar to those presented in Vafai and Kim[18]) showed that the numerical model predicts very accurately the velocity and temperature fields in a porous/fluid composite system.

Results and Discussion

As discussed earlier, the present problem is governed by six dimensionless parameters. These are the Darcy, Reynolds, two Prandtl numbers, inertia parameter, and A and B. In this section, the effects of these parameters on the flowfield, temperature field, and local Nusselt number distribution will be examined. The fixed input parameters that were used for all cases were $R = 1$, $l_1 = 6$, and $k_{\text{eff}}/k_f = 1$. Note that for illustrating the flow and temperature fields clearly, only part of the figures were presented. However, at all times, the much larger domain was used for numerical calculations and interpretation of the results. Furthermore, in this study the conductivity of the porous media is taken to be equal to that of fluid in order to concentrate on the effects of geometric and thermophysical variations. It should be noted that for the sake of brevity, the main features and characteristics of some of the results are only discussed and the corresponding figures are not presented. Figure 2 displays the effects of rectangular porous blocks on the fluid flow and convection heat transfer for a case where the Reynolds number is 750, Darcy number is 1×10^{-5}, inertia parameter is 0.35, Prandtl number is 0.7, the dimensionless height and width of the porous blocks are 0.25 and 1.0, respectively, and the spacing between the porous block is 1.

It should be noted that in the energy equation the transverse thermal dispersion has been embedded in the effective thermal conductivity term. In other words, the effective thermal conductivity in the energy equation is a combination of stagnant and dispersion transport mechanisms. Hence, the effective thermal conductivity can be decomposed into two parts; one stands for the stagnant thermal conductivity of the fluid-saturated porous medium, and the other incorporates the additional thermal transport due to the transverse mixing.[19]

Several interesting features are observed from these plots. The streamlines are considerably distorted in the channel due to the presence of the porous block array (Fig. 2a). The velocity distribution is parabolic at both the entrance and exit of the two plates. However, this distribution changes rapidly as the fluid encounters the porous block array, especially at the corners of block. As seen in Fig. 2, the blocks have a more prominent effect on the flow conditions downstream compared to the conditions upstream of the blocks. Another interesting feature is the formation of relatively large vortices behind each porous block separated by a small recirculation region rotating in a direction opposite to that of the larger vortices. The height of these recirculation regions is about twice the height of the porous blocks. A weak eddy is generated on the smooth upper plate surface corresponding to the reattached region on the bottom plate. The complicated flowfield within the channel is the result of four interrelated effects: 1) a penetrating effect pertaining to the porous medium, 2) a blowing effect caused by porous media displacing the fluid from the porous region into the fluid region, 3) a suction effect caused by the pressure drop behind the porous blocks resulting in a downward flow, 4) and the effect of boundary-layer separation. Therefore, the characteristic of the porous substrate plays a significant role on the flow and temperature fields. It should be noted that the presence of porous cavities in addition to the porous blocks creates various interesting effects for controlling the flowfield while augmenting the heat transfer. For example, the interactions between vortex flow inside the cavity and the external flow play a significant role in affecting the temperature field.[20]

The temperature field in the channel is displayed in Fig. 2c. As expected, the thickness of both upper and lower thermal boundary layers increases along the length of heated plates and becomes significantly distorted within and around the porous-block region. Also, the symmetric character of the temperature field re-establishes itself far enough downstream of the porous block region. The variation of local Nusselt number corresponding to the above temperature fields is illustrated in Fig. 2d. A periodic variation of Nusselt number on the bottom plate is observed starting before the leading edge of porous block array (from $x^* = 6$). The peak in each cycle occurs at an x value corresponding to the center of the larger vortex behind the porous block, while the minimum in each cycle occurs at around the location where the larger and the smaller vortices behind each block meet. The heat transfer in the rear part of each porous block is higher due to increased convection aided by higher velocities in the recirculation eddy. Whereas the heat transfer at around the location, where the larger and the smaller vortices meet, is lower due to an almost stagnant flowfield within that region. Comparison of local Nusselt number distributions for a channel with and without porous blocks shows that the recirculation flow caused by porous blocks can augment significantly the heat transfer rate.

Effect of the Darcy Number

The Darcy number is directly related to the permeability of the porous medium. The effect of variations in the Darcy number is depicted in Figs. 3 and 4 for $Re = 750$, $\Lambda = 0.35$, $Pr = 0.7$, $A = 4$, and $B = 1$, for $Da = 1 \times 10^{-5}$, 5×10^{-5}, and 9×10^{-5}. Comparison of the streamlines in Fig. 3 shows that the distortion of streamlines and the size of recirculation zones behind the porous blocks becomes less pronounced as the Darcy number increases. This in turn accelerates the core flow to satisfy the mass continuity and confines the development of recirculation zones in the transverse direction. For smaller Darcy numbers, the recirculation cell occupies only the space between the porous blocks and the flow penetration into the porous block array is significantly reduced. In the limit, if the Darcy number is reduced to a value approaching zero, there will be no streamlines penetrating the porous block and the flow passes over the solid block array. As the value of the Darcy number is reduced, the distortion of the isotherms becomes less pronounced. This is the direct result of the discussed flowfield. The variation of local Nusselt number for various Darcy numbers is displayed in Fig. 4. It is seen that the Darcy number has a significant impact on the local Nusselt number distribution. Here there is an interesting phenomenon for the overall trend in the Nusselt number distribution. There exists an optimum Darcy number corresponding to the largest

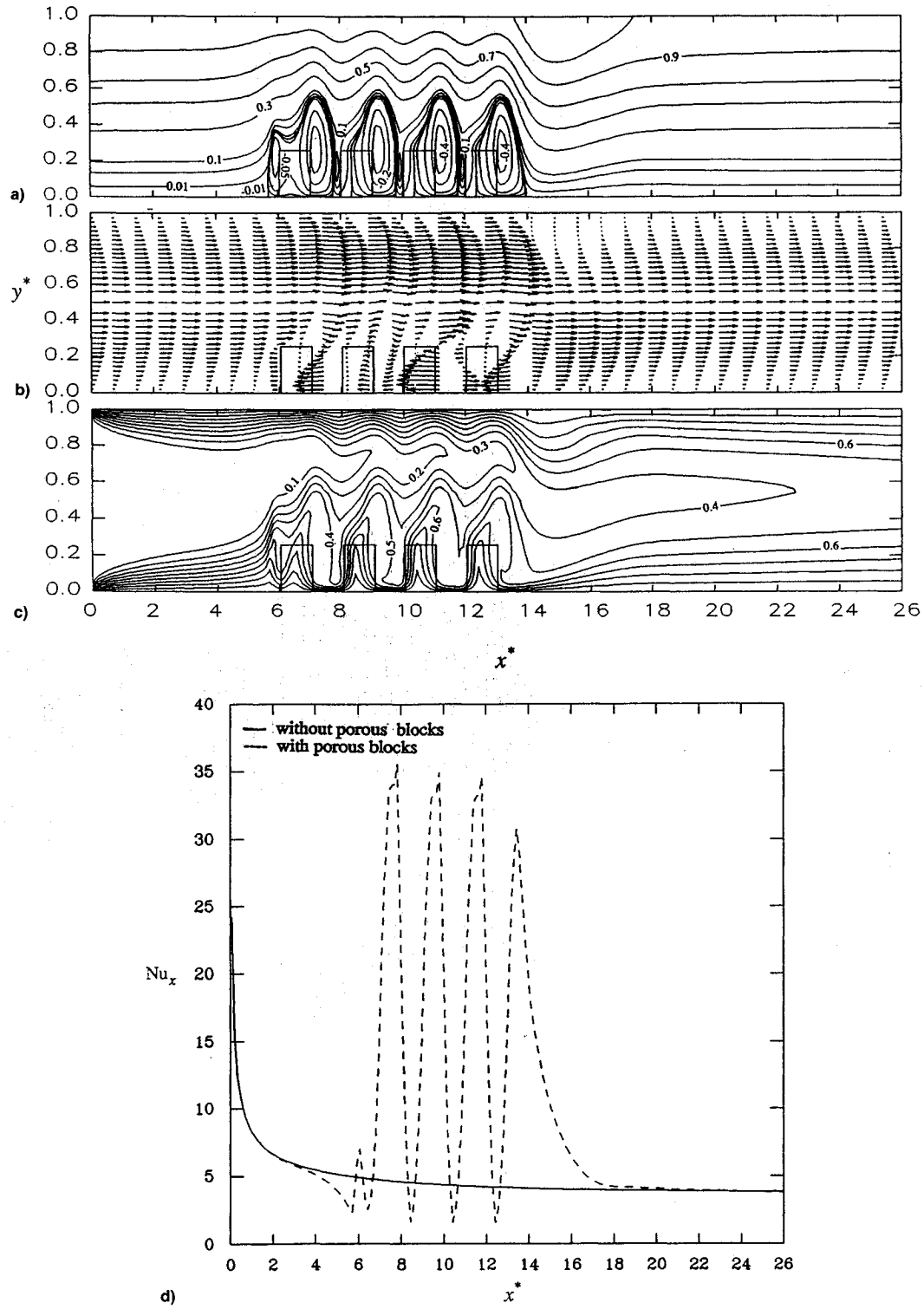

Fig. 2 Flow in a parallel plate channel with porous block obstacles for $Re = 750$, $Da = 1 \times 10^{-5}$, $\Lambda = 0.35$, $Pr = 0.7$, $k_{eff}/k_f = 1.0$, $A = 4$, $B = 1$, $H^* = 0.25$: a) streamlines, b) velocity distribution, c) isotherms, and d) local Nusselt number distribution.

values of the Nusselt number distribution. Below and above this optimum value the peak values of the Nusselt number drop off. This is the result of three competing effects. These are the flow through the porous blocks, the blowing effect, and the suction effect caused by the porous blocks.

Effect of Reynolds Number

Figures 5 to 6 show the streamlines and Nusselt number distribution for $Da = 1 \times 10^{-5}$, $\Lambda = 0.35$, $Pr = 0.7$, $A = 4$, and $B = 1$, with $Re = 750$, 1200, and 1500, respectively. It can be seen from Fig. 5 that increasing the Reynolds number from 750 to 1200 increases the distortion level in the core flow streamlines. As the Reynolds number increases, the larger vortex behind each block diminishes and ultimately vanishes. At the same time the size of the smaller vortex ahead of each block grows, occupying most of the porous block. For larger Reynolds numbers (>1200), a large recirculation region is formed behind the last porous block. The reason for this is that at these larger Reynolds numbers a very sharp velocity gradient occurs at the right top corner of the last porous block, which delays the reattachment of the core flow to the bottom plate. As expected, the temperature fields corresponding to different Reynolds numbers show that at higher Reynolds numbers the extent of distortion for isotherms increases. The

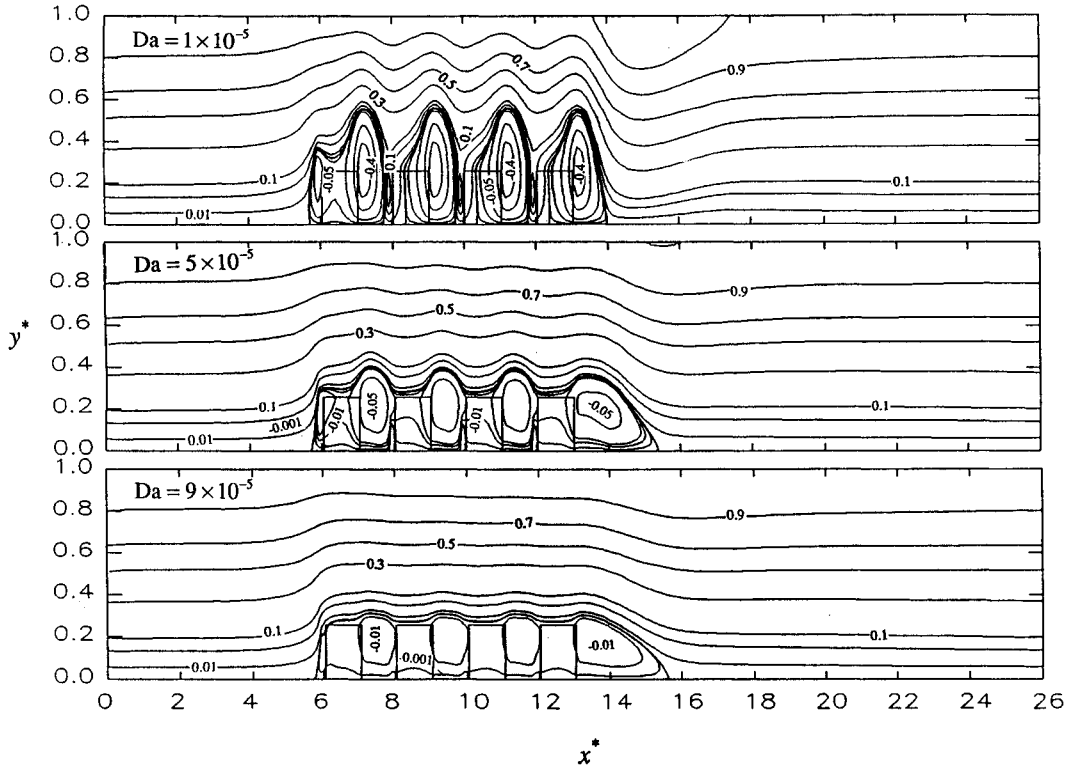

Fig. 3 Effects of the Darcy number on streamlines for flow in a parallel plate channel with porous block obstacles for Re = 750, Λ = 0.35, A = 4, B = 1, H^* = 0.25.

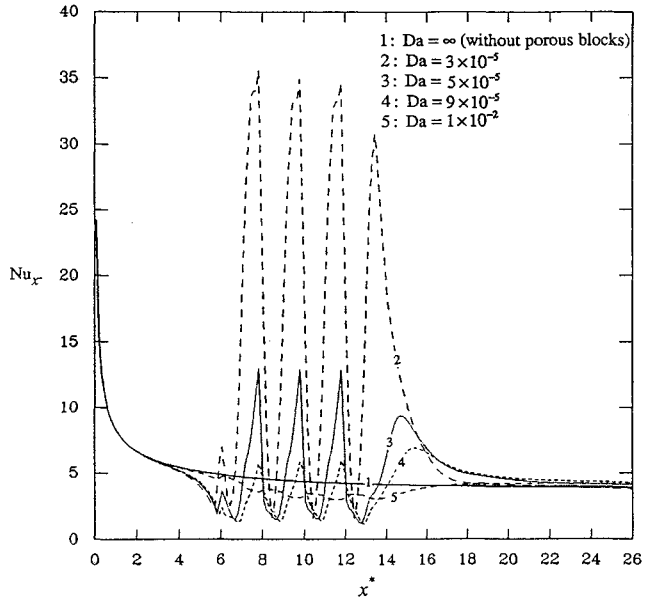

Fig. 4 Effects of the Darcy number on local Nusselt number distribution for flow in a parallel plate channel with porous block obstacles for Re = 750, Λ = 0.35, Pr = 0.7, k_{eff}/k_f = 1.0, A = 4, B = 1, H^* = 0.25.

effect of the Reynolds number on the local Nusselt number distribution is depicted in Fig. 6. It shows that both peak and trough values of Nu_x increase with an increase in the Reynolds number. The peak values of the Nusselt numbers correspond to the reattachment regions of the core flow to the external boundary behind each porous block, which increases the heat transfer by convection. It should be noted that a high rate of increase in the overall rate of heat transfer from the channel into the flow can be attained by using the porous blocks.

Inertial Effects

The effect of an increase or decrease in the inertial parameter is shown in Figs. 7 and 8 for Re = 1500, $Da = 1 \times 10^{-5}$, Pr = 0.7, A = 4, and B = 1, for Λ = 0.35, 21, and 35. The flowfields displayed in Fig. 7 reveal that as the inertial parameter increases, the vortex behind each block gradually grows inside the interblock spacing. This is due to the larger bulk frictional resistance that the flow encounters at larger values of the inertial parameter. This in turn causes a larger blowing effect through porous blocks, which displaces the fluid deeper into the core flow, and creates a larger recirculation in the right top corner of porous blocks after encountering the primary flowfield. As expected, the distortion in the isotherms becomes pronounced as the inertial parameter increases due to the increase in the size of the vortices behind the porous blocks. Again, this is the direct result of larger blowing effect for a larger inertial parameter. Figure 8 shows the variation of Nu_x with inertial parameter. In general, as the inertial parameter increases, the peak value of Nu_x increases. This is due to the larger fluid mixing caused by a larger recirculation zone for larger values of the inertial parameter.

Prandtl Number Effects

In order to determine the effect of the Prandtl number on the flow and temperature fields, three different Prandtl numbers were compared such that they will cover a wide range of thermophysical properties. These comparisons, shown in Fig. 9, were performed for Re = 750, $Da = 1 \times 10^{-5}$, Λ = 0.35, A = 4, and B = 1, for three different fluids with Pr = 0.7 (air), Pr = 7 (water), and Pr = 100 (typical value for oil), respectively. Since Re, Da, and Λ are fixed, the variation of Prandtl number has no effect on the flowfield, and therefore, the flowfield is the same for all Prandtl numbers. This flowfield is shown in Fig. 2a. As expected, increasing the Prandtl number decreases the thickness of the thermal boundary layer. As seen in Fig. 9, the local Nusselt number and its fluctuations increase with an increase in the Prandtl number.

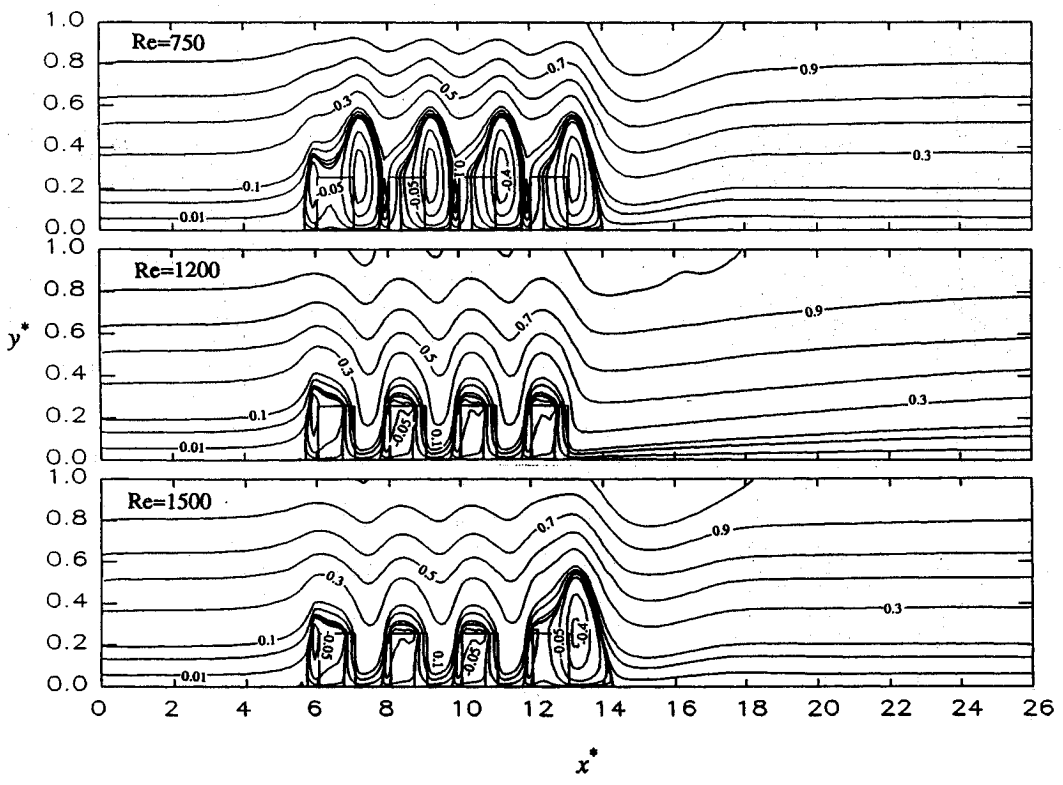

Fig. 5 Effects of the Reynolds number on streamlines for flow in a parallel plate channel with porous block obstacles for $Da = 1 \times 10^{-5}$, $\Lambda = 0.35$, $A = 4$, $B = 1$, $H^* = 0.25$.

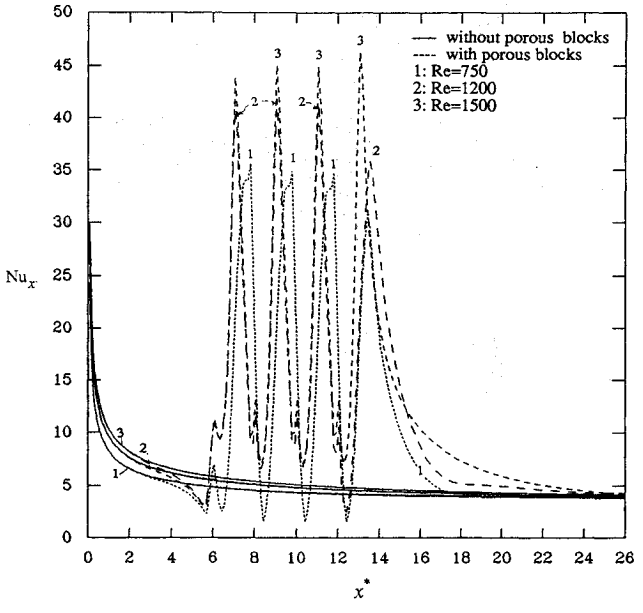

Fig. 6 Effects of the Reynolds number on local Nusselt number distribution for flow in a parallel plate channel with porous block obstacles for $Da = 1 \times 10^{-5}$, $\Lambda = 0.35$, $Pr = 0.7$, $k_{eff}/k_f = 1.0$, $A = 4$, $B = 1$, $H^* = 0.25$.

Note that utilizing a combination of Re and Pr alone (i.e., $Pe = RePr$) is insufficient for depicting the temperature field or describing Nusselt number correlations.

Effect of A and B

A and B are related to the porous block's aspect ratio and pitch. The effect of aspect ratio on the flow and temperature fields were studied for $Re = 750$, $Da = 1 \times 10^{-5}$, $\Lambda = 0.35$, $Pr = 0.7$, and $B = 1$. The streamlines for $A = 4$ and $A = 8$ are represented on Fig. 10. As can be seen in Fig. 10, when the value of A is increased from 4 to 8, the distortions for streamlines and isotherms become less pronounced. In addition, the size of recirculation and interaction between successive porous blocks reduce. This is due to the relative decrease in the height of the porous blocks, which in turn offers a lower degree of obstruction to the flow for larger values of A.

The effect of pitch on flow and temperature fields was investigated for a case where $Re = 750$, $Da = 1 \times 10^{-5}$, $\Lambda = 0.35$, $Pr = 0.7$, and $A = 4$, for $B = 3$, 2, and 1. For larger values of the pitch parameter, the recirculation zones caused by the porous blocks are relatively independent of each other. At the same time, several eddies are generated on the upper smooth plate due to the core flow attaching to the bottom plate between the blocks. With decreasing pitch up to $B = 2$, recirculation zones behind the first and second porous blocks vanish. Comparison of the temperature fields shows that as the pitch decreases from $B = 3$ to $B = 2$, the isotherms are more distorted. However, as B further decreases to 1, the distortion of the isotherms is less pronounced.

Effects of the Porous Blocks on the Pressure Drop

In the stream function-vorticity formulation, the pressure field is eliminated in obtaining the solution. However, the pressure field can be recovered from the converged stream function and vorticity fields. This is done by integrating the pressure gradient along the upper plate wall. The pressure gradient is derived from the momentum equation utilizing the impermeable boundary conditions on the solid wall. Since $u^* = 0$ and $v^* = 0$ on the upper plate, the pressure gradient on that surface casted in dimensionless form can be presented as

$$\left.\frac{\partial p^*}{\partial x^*}\right|_{y^*=1} = -\frac{1}{Re}\left.\frac{\partial \xi^*}{\partial y^*}\right|_{y^*=1} \tag{20}$$

where pressure p^* is nondimensionalized with respect to

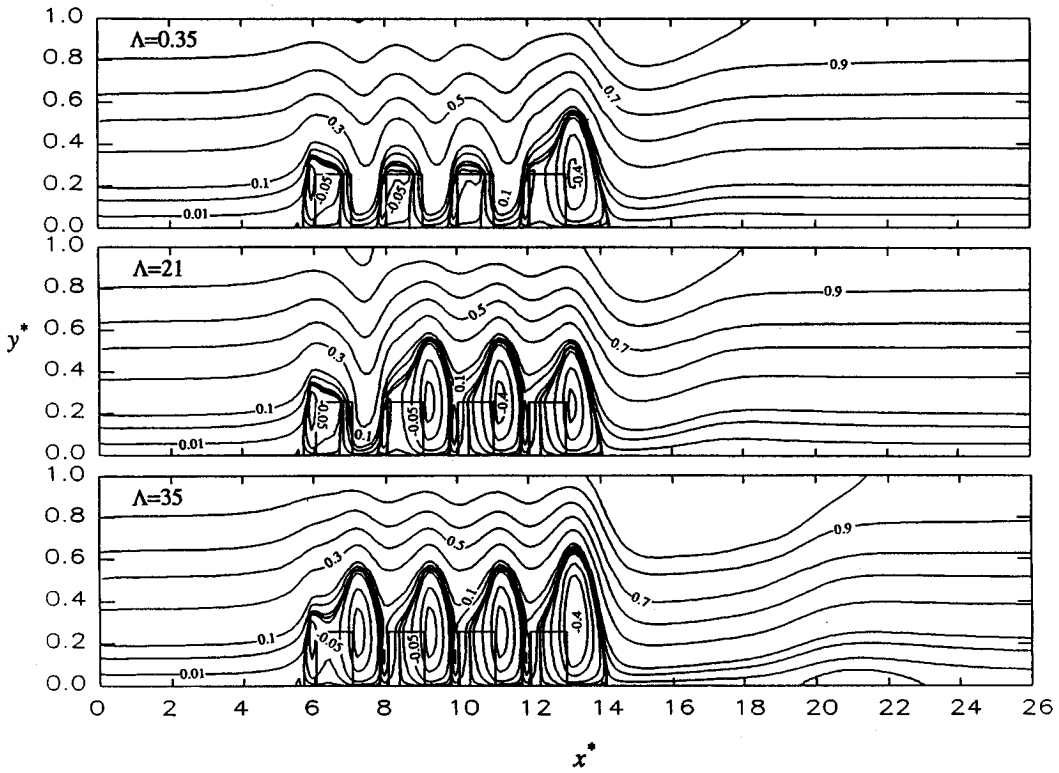

Fig. 7 Influence of the inertial parameter on streamlines for flow in a parallel plate channel with porous block obstacles for $Re = 1500$, $Da = 1 \times 10^{-5}$, $A = 4$, $B = 1$, $H^* = 0.25$.

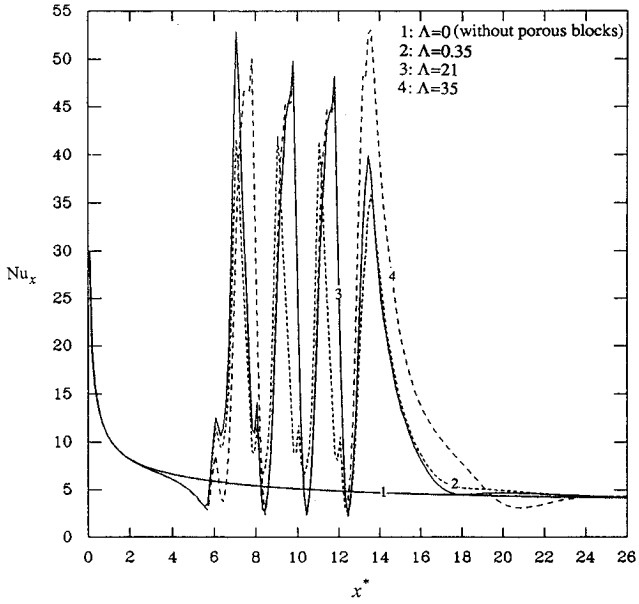

Fig. 8 Influence of the inertial parameter on local Nusselt number distribution for flow in a parallel plate channel with porous block obstacles for $Re = 1500$, $Da = 1 \times 10^{-5}$, $Pr = 0.7$, $k_{eff}/k_f = 1.0$, $A = 4$, $B = 1$, $H^* = 0.25$.

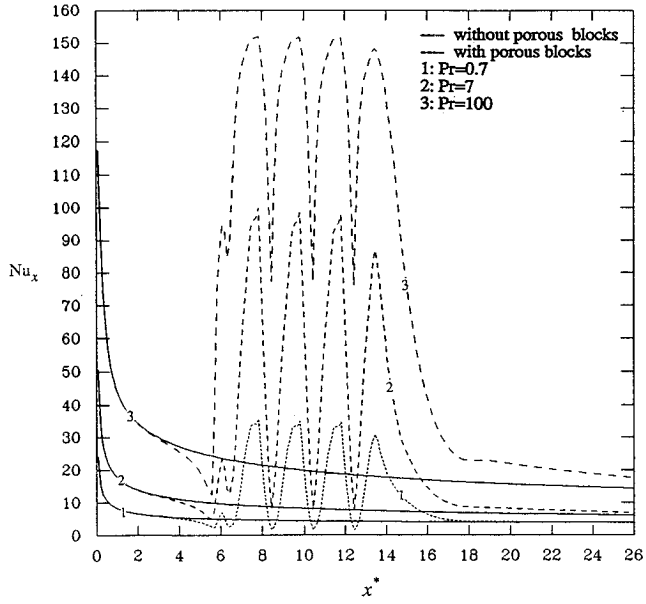

Fig. 9 Prandtl number effects on local Nusselt number distribution for flow in a parallel plate channel with porous block obstacles for $Re = 750$, $Da = 1 \times 10^{-5}$, $\Lambda = 0.35$, $k_{eff}/k_f = 1.0$, $A = 4$, $B = 1$, $H^* = 0.25$.

ρu_{av}^{*2}. The total pressure drop along the upper plate wall is then obtained from

$$\frac{p_L^* - p_0^*}{\rho u_{av}^{*2}} = \int_0^{L^*} \left.\frac{\partial p^*}{\partial x^*}\right|_{y^*=1} dx^* = \int_0^{L^*} -\frac{1}{Re}\left.\frac{\partial \xi^*}{\partial y^*}\right|_{y^*=1} dx^* \tag{21}$$

where P_0 refers to the inlet pressure condition.

Figure 11 shows the effect of the Reynolds number on the pressure distribution along the upper plate wall for a channel with and without the porous blocks. It can be seen that the porous block array causes an increase in the total pressure drop. The reason is that as the flow approaches the smaller passage formed by the porous block and the upper surface of the channel, the fluid starts to accelerate, resulting in an increase in the pressure drop. Pressure recovery behind each porous block is not complete due to pressure loss in the recirculation zones. Note that the linear feature of the curve at a downstream position indicates a seemingly fully developed

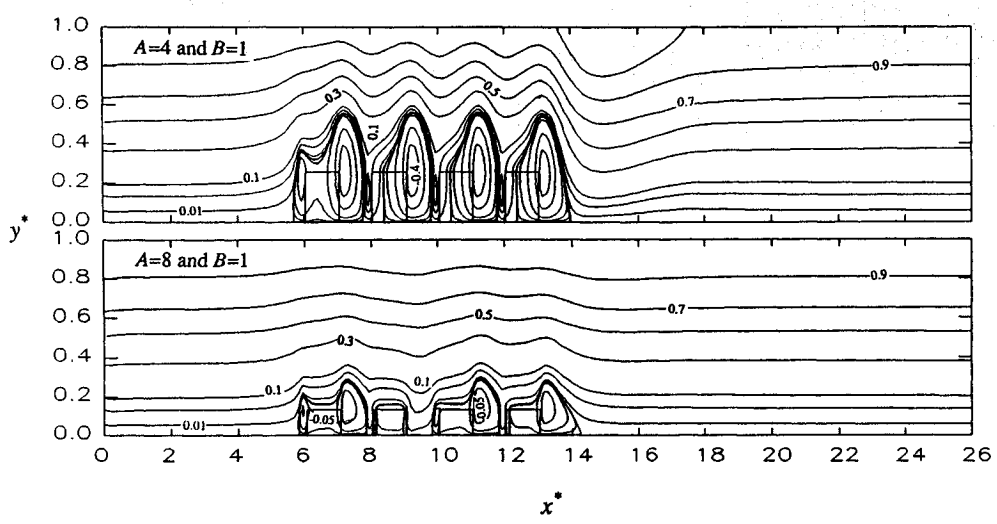

Fig. 10 Influence of the geometric parameter A on streamline and isotherms for flow in a parallel plate channel with porous block obstacles for $Re = 750$, $Da = 1 \times 10^{-5}$, $\Lambda = 0.35$, $Pr = 0.7$, $k_{eff}/k_f = 1.0$, $B = 1$, $H^* = 0.25$.

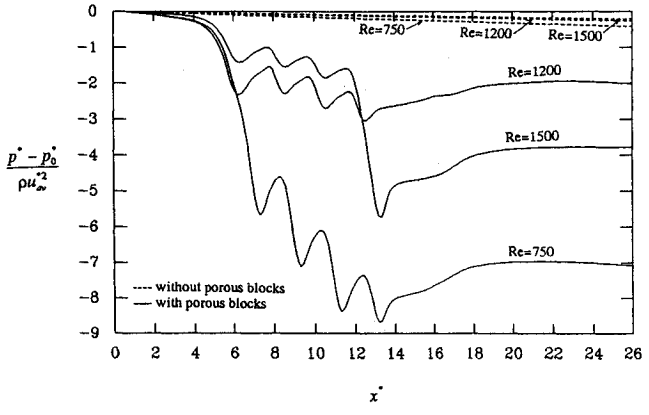

Fig. 11 Effects of the Reynolds number on the pressure drop along the upper plate for $Da = 1 \times 10^{-5}$, $\Lambda = 0.35$, $A = 4$, $B = 1$, $H^* = 0.25$.

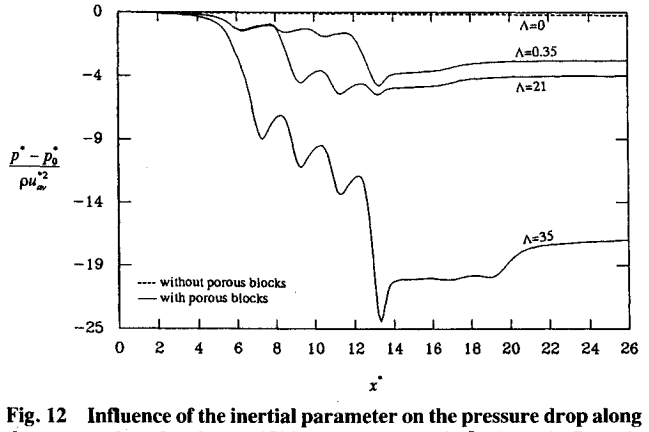

Fig. 12 Influence of the inertial parameter on the pressure drop along the upper plate for $Re = 1500$, $Da = 1 \times 10^{-5}$, $A = 4$, $B = 1$, $H^* = 0.25$.

character. For the case without the porous blocks (smooth channel) the fully developed velocity profile is used, that is

$$\left.\frac{\partial p^*}{\partial x^*}\right|_{y^*=1} = -\frac{1}{Re}\left.\frac{\partial^2 u^*}{\partial y^{*2}}\right|_{y^*=1} = -\frac{12}{Re} \qquad (22)$$

The pressure drop for the smooth channel will actually be more than what is predicted by the above equation due to entry length effect. The inverse proportionality of the pressure drop and the Reynolds number for a smooth channel can be

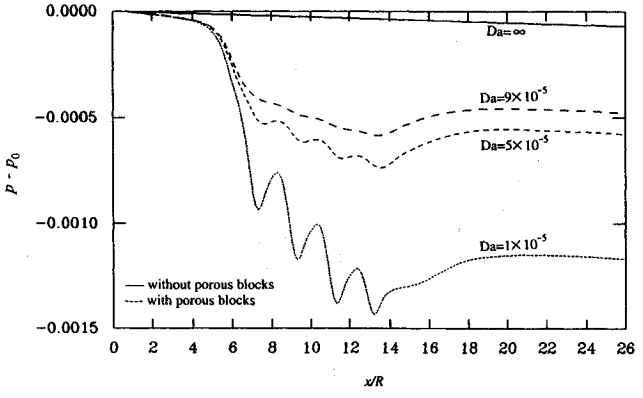

Fig. 13 Effects of the Darcy number on the pressure drop along the upper plate for $Re = 750$, $\Lambda = 0.35$, $A = 4$, $B = 1$, $H^* = 0.25$.

observed in Fig. 11. As expected, for the smooth channel the dimensional pressure drop increases with an increase in the Reynolds number. However, for the channel with porous obstacles, the dimensional pressure drop is larger for $Re = 750$ than for $Re = 1200$. This is due to the absence of the large recirculation region formed behind the last porous block for $Re = 1200$, resulting in a smaller pressure loss. This interesting phenomena clearly shows that the porous blocks can be optimized for different applications.

Pressure drop increases with the inertial number, as shown in Fig. 12. This is due to the fact that the rate of pressure drop increases across the larger recirculation zones. In addition, the larger eddy on the upper plate delays the pressure recovery behind the last porous block. The influence of Darcy number on the magnitude of the pressure drop along the upper plate is displayed in Fig. 13. It can be seen that the computed pressure distribution becomes more distorted across the porous block array for lower Darcy number. This is due to stronger vorticity gradients which exist for lower Darcy numbers. It should be noted that the Prandtl number has no effect on the flowfield or the pressure drop distribution along the upper plate.

Conclusions

A detailed investigation of forced convection augmentation in a channel using multiple emplaced porous blocks has been presented. The Brinkman-Forchheimer-extended Darcy model was used for the porous media. The rectangular porous blocks change the incoming parabolic velocity field considerably, resulting in the formation of vortices penetrating these porous blocks. These vortices which can be controlled by altering

some governing parametric values have significant effects on the heat transfer characteristics. The effects of the Reynolds numbers, Darcy numbers, inertial parameters, Prandtl numbers, and geometric parameters on forced convection enhancement in a channel using multiple emplaced porous blocks have been analyzed in detail, and the existence of an optimum porous matrix is demonstrated. Comparison of the local Nusselt number distributions between the channel with and without porous blocks clearly shows that significant heat transfer augmentation can be achieved through the emplacement of porous blocks.

Acknowledgment

The support of DOE under Grant DE-FG02-93ER61612 for part of this work is acknowledged and appreciated.

References

[1]Koh, J. C. Y., and Colony, R., "Analysis of Cooling Effectiveness for Porous Material in a Coolant Passage," *Journal of Heat Transfer*, Vol. 96, Series C, No. 3, 1974, pp. 324–330.

[2]Koh, J. C. Y., and Stevens, R. L., "Enhancement of Cooling Effectiveness by Porous Material in Coolant Passage," *Journal of Heat Transfer*, Vol. 97, Series C, No. 2, 1975, pp. 309–311.

[3]Rohsenow, W. M., and Hartnett, J. P., *Handbook of Heat Transfer*, McGraw-Hill, New York, 1973.

[4]Kaviany, M., "Laminar Flow Through a Porous Channel Bounded by Isothermal Parallel Plates," *International Journal of Heat and Mass Transfer*, Vol. 28, No. 4, 1985, pp. 851–858.

[5]Vafai, K., and Tien, C. L., "Boundary and Inertia Effects on Flow and Heat Transfer in Porous Media," *International Journal of Heat and Mass Transfer*, Vol. 24, No. 2, 1981, pp. 195–203.

[6]Poulikakos, D., and Renken, K., "Analysis of Forced Convection in a Duct Filled with Porous Media in Heat Transfer," *Heat Transfer in Geophysical and Geothermal Systems*, Vol. 76, American Society of Mechanical Engineers HTD, 1987, pp. 9–20.

[7]Beavers, G. I., and Joseph, D. D., "Boundary Conditions at a Naturally Permeable Wall," *Journal of Fluid Mechanics*, Vol. 30, Pt. 7, 1967, pp. 197–207.

[8]Levy, T., and Sanchez-Palencia, E., "On Boundary Conditions for Fluid Flow in Porous Media," *International Journal of Engineering Science*, Vol. 13, No. 11, 1975, pp. 923–940.

[9]Vafai, K., and Thiyagaraja, R., "Analysis of Flow and Heat Transfer at the Interface Region of a Porous Medium," *International Journal of Heat and Mass Transfer*, Vol. 30, No. 7, 1987, pp. 1391–1405.

[10]Poulikakos, D., and Kazmierczak, K. M., "Forced Convection in a Duct Partially Filled with a Porous Material," *Journal of Heat Transfer*, Vol. 109, No. 3, 1987, pp. 653–662.

[11]Ichimiya, K., and Mitsushiro, K., "Enhancement of the Heat Transfer of Wide Temperature Range in a Narrow Flow Passage," *Experimental Heat Transfer, Fluid Mechanics and Thermodynamics*, Elsevier, 1988, pp. 659–664.

[12]Kaviany, M., "Boundary Layer Treatment of Forced Convection Heat Transfer from a Semi-Infinite Flat Plate Embedded in Porous Media," *Journal of Heat Transfer*, Vol. 109, No. 2, 1987, pp. 345–349.

[13]Kelkar, K. M., and Patankar, S. V., "Numerical Prediction of Flow and Heat Transfer in a Parallel Plate Channel with Staggered Fins," *Journal of Heat Transfer*, Vol. 109, No. 1, 1987, pp. 25–30.

[14]Adams, J., and Ortega, J. A., "A Multicolor SOR Method for Parallel Computation," *Proceedings of Int. Conf. on Parallel Procession*, 1982, pp. 53–56.

[15]Patankar, S. V., *Numerical Heat Transfer and Fluid Flow*, Hemisphere, 1980.

[16]Lundgren, T. S., "Slow Flow Through Stationary Random Beds and Suspensions of Spheres," *Journal of Fluid Mechanics*, Vol. 51, Pt. 2, 1972, pp. 273–299.

[17]Neale, G., and Nader, W., "Practical Significance of Brinkman's Extension of Darcy's Law Coupled Parallel Flows Within a Channel and a Bounding Porous Medium," *Canadian Journal of Chemical Engineering*,Vol. 52, No. 4, 1974, pp. 475–478.

[18]Vafai, K., and Kim, S. J., "Analysis of Surface Enhancement by a Porous Substrate," *Journal of Heat Transfer*, Vol. 112, No. 3, 1990, pp. 700–705.

[19]Cheng, P., "Heat Transfer in Geothermal System," *Advances in Heat Transfer*, Vol. 14, 1978, pp. 1–105.

[20]Huang, P. C., and Vafai, K., "Internal Heat Transfer Augmentation in a Parallel Plate Channel Using an Alternate Set of Porous Cavity-Block Obstacles," *Numerical Heat Transfer* (to be published).